RESEARCH PAPER

VARIATION OF AEROSOL PROPERTIES BASED ON SATELLITE DATA OVER THE STUDY AREA OF LHAASO

Andleeb Masood[1*], Fengrong. Zhu[1], Zulfaqar Sa'adi[2], Irfan Ullah[3], Md. Abdullah Al Mamun Hridoy[4], Huan-Yu Jia[1]

[1]School of Physical Science and Technology, Southwest Jiaotong University, Chengdu, 611756, China
[2]Centre for Environmental Sustainability and Water Security, Research Institute for Sustainable Environment, Universiti Teknologi Malaysia, UTM Skudai, Johor Bahru, 81310, Malaysia
[3]College of Hydrology and Water Resources, Hohai University, Nanjing, Jiangsu, 210098.China
[4]Department of Fish Biology and Genetics, Faculty of Fisheries, Sylhet Agricultural University, Sylhet-3100, Bangladesh
***Corresponding author:** andleebmasood238@gmail.com
Received: April 2ndt 2025 / Accepted: February 26th 2026 / Published: March 31st 2026
https://doi.org/10.24057/2071-9388-2026-4063

ABSTRACT. Atmospheric aerosols play a crucial role in modulating Earth's radiation balance and climate systems, yet they remain a major source of uncertainty in climate modeling. This study aims to characterize aerosol dynamics over the Large High Altitude Air Shower Observatory (LHAASO; 29.36° N, 100.14° E; ~4,410 m above sea level) region by analyzing satellite-based measurements of Aerosol Optical Depth (AOD), Aerosol Index (AI), Single Scattering Albedo (SSA), and Extinction Coefficient (EC) from Moderate Resolution Imaging Spectroradiometer (MODIS), Sentinel-5P, CALIPSO, OMI, and MERRA-2 Reanalysis for the period 2017–2023. The mean AOD peaked at 0.24 ± 0.02, primarily due to long-range dust transport from the Taklamakan and Gobi deserts. The AI varied between 0.68 and 1.26 (standard deviation SD = 0.31 ± 0.26), indicating moderate to significant aerosol activity, particularly during dust events. Aerosol mass concentration (MC) ranged from 4.14 to 31.07 μg/m^3 with a SD of 0.67 ± 8.14, reflecting influences from dust transport, meteorological conditions, and local emissions. The EC generally decreased with altitude, consistent with reduced aerosol concentrations and particle sizes. These findings advance our understanding of aerosol behavior in complex terrain and provide essential perspectives for improving climate projections and radiative forcing assessments.

KEYWORDS: Aerosol index, AOD, Extinction coefficient, Satellite remote sensing

CITATION: Masood A., Zhu F., Sa'adi Z., Ullah I., Md. Abdullah Al Hridoy M., Huan-Yu Jia (2026). Variation Of Aerosol Properties Based On Satellite Data Over The Study Area Of LHAASO. Geography, Environment, Sustainability, 1 (19), 115-129
https://doi.org/10.24057/2071-9388-2026-4063

ACKNOWLEDGEMENTS: This work was supported by the National Key R&D Program of China (2021YFA0718403) and the National Natural Science Foundation of China for International Scientists under Grant No. 42350410438. We acknowledge the NASA Langley Research Center Atmospheric Sciences Data Center.

Conflict of interests: The authors reported no potential conflict of interests.

INTRODUCTION

The prediction of global climate change is hindered by significant uncertainties arising from the highly variable spatio-temporal distribution of atmospheric aerosols and our limited understanding of their optical properties (IPCC 2023). In the atmosphere, tiny suspended particles known as aerosols range in size from approximately 0.001 to 100 μm (Mahowald et al. 2014). These particles exist in various types, including intermediate, fine, and coarse modes, depending on their dimensions. Aerosols influence solar radiation by scattering and absorbing it, with their impact varying based on their chemical composition and size (Delene & Ogren 2002; Gautam et al. 2021; Jacobson 2002). By interacting with radiation, aerosols affect the Earth's radiation budget both spatially and temporally, a process known as radiative forcing. This alters the Earth's radiative balance and impacts the global climate (Ramachandran et al. 2006; Ranjan et al. 2007; Satheesh & Ramanathan, 2000). Due to their short lifespans and uneven geographic distribution, which is influenced by emissions (Bhowmik et al. 2025), atmospheric chemical reactions, and weather patterns, aerosol properties exhibit significant spatial and temporal variability (Andrews et al. 2011; Boucher et al. 2013; Kumar et al. 2022b; Park et al. 2019). Submicron-sized aerosols may also play a key role in the formation of mist and fog in certain locations (Lillis et al. 1999). Aerosols interact with solar radiation directly through scattering and absorption, while their indirect effects involve influencing cloud processes. Studying aerosols not only deepens researchers' understanding of their environmental effects but also offers essential theoretical support for decision-makers in developing effective environmental protection policies (Edenhofer & Seyboth, 2013; Gong et al. 2015; Zhang et al. 2014a).

Aerosol Optical Depth (AOD) is the fundamental optical property of atmospheric aerosols, serving as a key indicator

of atmospheric clarity. It plays a critical role in characterizing atmospheric turbidity and is essential for assessing the effects of aerosols on climate (Zhang et al. 2014b). AOD is frequently used in studies that examine how aerosols influence regional climate's spatial and temporal variation in atmospheric characteristics (Jing et al. 2018; Wang et al. 2019). Moderate Resolution Imaging Spectroradiometer (MODIS) AOD products produce high retrieval accuracy, extensive time series, and excellent spatial coverage. These attributes have been validated through numerous studies conducted by international researchers, highlighting their significant value in aerosol research (Jie et al. 2017; Perumpully, Gautam, & M, 2024; Tian et al. 2018). In recent years, the escalating environmental challenges in China have prompted researchers to intensively investigate the optical, physical, and distribution characteristics of aerosols across key developed regions, including the Yangtze River Delta, Beijing-Tianjin-Hebei, and the Pearl River Delta (Bilal et al. 2019; Zhao et al. 2023). On the other hand, the Beijing urban area helps assess the efficacy of clean air action and provide crucial optical parameters for assessing radiative forcing within two size ranges (Hu et al. 2023; Ren et al. 2022; Zhao et al. 2019). The accurate monitoring of aerosol optical and physical characteristics and their spatiotemporal distributions over the Large High Altitude Air Shower Observatory (LHAASO) holds significant practical implications for atmospheric environmental protection.

Satellite remote sensing (SRS) is essential, as it enables the global measurement of highly variable aerosol fields over extended periods (Blaga & Gautam, 2024; Gautam et al. 2024; Ginoux et al. 2004; Perumpully & Gautam 2025). However, despite advancements in satellite observation techniques for aerosols facilitated by the utilization of increasingly sophisticated instruments, discrepancies persist among various satellite products, indicating ongoing inaccuracies in SRS techniques (Hridoy & Paul 2024). Satellite sensors often have limited spatial resolution, which can hinder the ability to detect fine-scale aerosol features and variability. Hence, a comprehensive analysis of the optical properties and other attributes of aerosols cannot be achieved solely using existing satellite data. The LHAASO study area, because of its distinctive high-altitude environment, is fundamental for understanding the spatial and temporal variations of aerosol properties. The findings of this study are expected to contribute to a deeper understanding of aerosol dynamics in high-altitude regions and provide valuable insights for improving climate models, air quality forecasts, and environmental management strategies. The main objective of this study is to examine aerosol properties using satellite data collected over LHAASO for an extended period (~7 years), considering variations across all four seasons. In this study, we used all available satellite data from 2017 to 2023 to analyze AOD, aerosol index (AI), aerosol extinction coefficient (EC), aerosol concentration, single scattering albedo (SSA), dust surface density, and dust mass concentration.

MATERIALS AND METHODS

The datasets were integrated through a pixel-to-station matching procedure, with explanatory weights determined statistically rather than assigned arbitrarily. Errors in satellite data were minimized through atmospheric correction, cloud masking, and validation against in situ measurements using root-mean-square error (RMSE) and bias statistics. Preprocessing included filling small gaps in the measurement series using linear interpolation between adjacent time points, filtering unreliable satellite pixels flagged by quality assurance bands, and removing spurious ground measurements outside instrument calibration ranges. Outliers were detected via the interquartile range method and excluded only when confirmed as artifacts (e.g., sensor malfunction or accidental contamination), to ensure the dataset reflected genuine environmental variability.

Site Description

The study area encompasses LHAASO (29.35°N, 100.13°E, 4,410.0 m a.s.l.) situated within the Hengduan Mountains. These mountains serve as the junction between the southeastern edge of the Tibetan Plateau, the Yunnan-Guizhou Plateau, and the Sichuan Basin. With an average elevation of 4,410 m a.s.l., the Hengduan Mountains represent a unique and sensitive ecological zone. The location map of LHAASO is presented in Fig. 1. The lack of readily available data collection has hindered comprehensive analysis of AOD dynamics in the area. Despite sporadic ground-based measurements historically recorded at sites like Yunling Baimang Snow Mountain and the Shangri-La atmosphere background station, there exists a gap in continuous monitoring. Recent efforts, including ground measurements conducted at the Litang station, approximately 70 km from LHAASO (Masood et al. 2025), have started shedding light on AOD variations, particularly during the summer months. The elevation map of the study area reveals a diverse topography characterized by significant variations in altitude, as shown in Fig. 2. Spanning from a towering 4,883 m at its highest point to a lower elevation of 4,036 m at its lowest, the map showcases the rugged terrain of the region. These elevation fluctuations play a crucial role in shaping local climate patterns, hydrological processes, and ecosystem dynamics. The depiction of such elevation gradients underscores the importance of understanding the spatial context in which AOD variations occur. As aerosols interact with the atmosphere, their impact can be influenced by the complex interplay of altitude, terrain features, and atmospheric conditions. Therefore, integrating elevation data into the analysis provides valuable information for the spatial distribution and potential drivers of AOD across the study area. Digital Elevation Models (DEMs) with a 30 m resolution were used to establish a comprehensive understanding of the terrain. These DEMs, sourced from the Shuttle Radar Topography Mission (SRTM) through the USGS Earth Explorer platform, allowed for precise calculation and visualization of the elevation profile surrounding the LHAASO observatory.

Data Acquired

The study relied on a multi-satellite and reanalysis approach, where each dataset contributed complementary aerosol-related parameters. Rather than applying fixed weights, the datasets were integrated according to their specific strengths: MODIS for spatially extensive AOD, Sentinel-5P for high-resolution AI, CALIPSO for vertical extinction profiles, OMI for single scattering albedo, and MERRA-2 for dust concentration estimates. Inter-comparison between overlapping parameters (e.g., MODIS AOD with Sentinel-5P AI) was used to ensure consistency. Satellite retrieval errors, particularly those influenced by surface reflectance and cloud contamination, were minimized through preprocessing, quality flag filtering, and validation against MERRA-2 reanalysis.

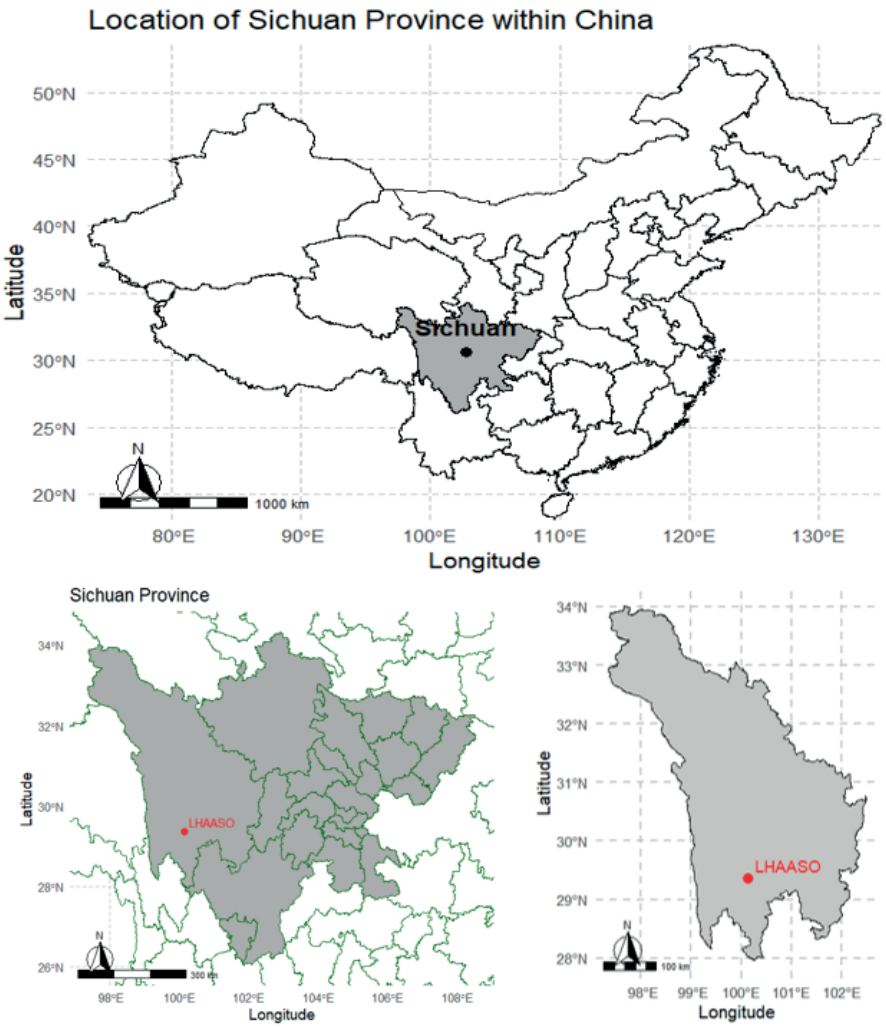

Fig. 1. Location of the LHAASO site within Sichuan Province, China. Sichuan Province highlighted within the map of China (top). Administrative boundaries of Sichuan Province with the LHAASO site marked (bottom left). Enlarged view showing the precise location of LHAASO within Sichuan (bottom right)

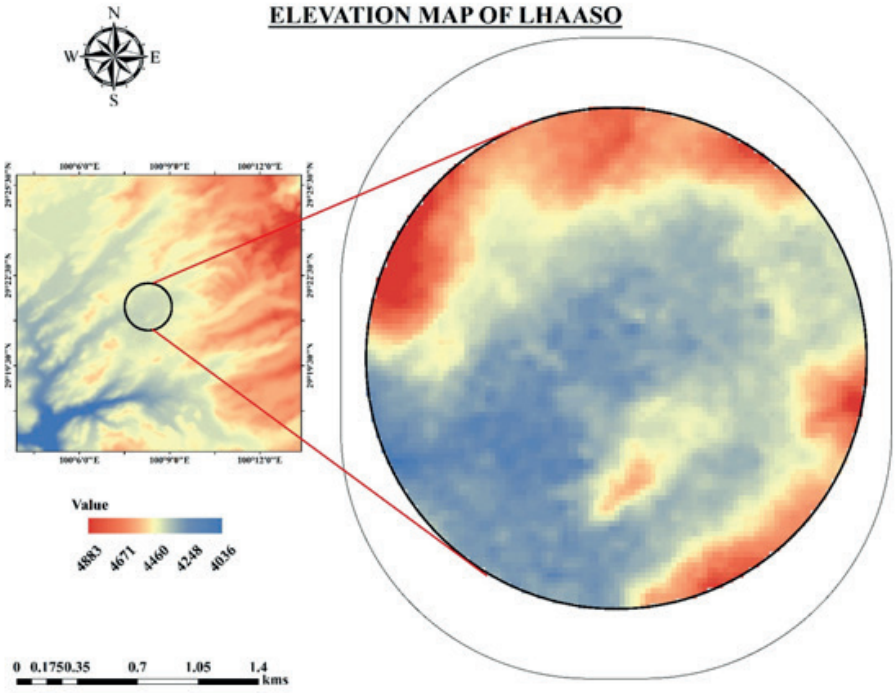

Fig. 2. Digital Elevation Map of LHAASO. The map was created with ArcGIS (version 10.8[1])

[1]https://www.arcgis.com/

MODIS

National Aeronautics and Space Administration (NASA)'s Earth Observing System (EOS) launched the Terra and Aqua satellites to monitor the Earth's properties, including the atmosphere and oceans. The Moderate Resolution Imaging Spectroradiometer (MODIS), a key instrument on the Terra satellite, has provided highly accurate observations of aerosols and clouds since its operation began in February 2000. MODIS is renowned for its exceptional spatio-temporal resolution, as it measures radiation reaching the top of the atmosphere across 36 spectral channels, ranging from 0.41 µm to 14.2 µm. The instrument has a wide swath of 2,330 km, with spatial resolutions of 250 m, 500 m, and 1,000 m, and offers a temporal resolution of 1 to 2 days. Alam et al. (2014) found that MODIS's capability to track various fluctuations and compile data has enhanced scientists' understanding of atmospheric, terrestrial, and oceanic phenomena. This accumulated data is invaluable for investigating aerosol characteristics and understanding aerosol–cloud interactions. Using the Deep Blue algorithms (Hridoy et al. 2025), the MODIS instrument aboard the Terra satellites provides comprehensive global coverage of aerosol optical properties over land. The Level 3 MODIS Terra data (MYD08_D3v6) of Aerosol Optical Depth (AOD) used during the period from 2017 to 2023 is retrieved from the Giovanni website[2]. Fig. 3 shows the range of AOD and Aerosol Index (AI) over the LHAASO region from 2017 to 2023.

Sentinel-5P

The Sentinel-5 Precursor (Sentinel-5P) satellite, part of the European Space Agency's Copernicus program, is indeed essential for monitoring atmospheric composition, including aerosol properties through the AI. The AI serves as a quantitative measure that assesses the presence and distribution of aerosols in the atmosphere, providing crucial insights into air quality and climate change. Sentinel-5P Near Real-Time ultraviolet (UV) AI data was incorporated into the analysis. It offers detailed examination of aerosol concentrations and distributions within the study region.

CALIPSO

The Cloud-Aerosol Lidar and Infrared Pathfinder Satellite Observations (CALIPSO) mission is a collaborative effort between NASA's Langley Research Center (LaRC) and the National Space Research Center of France, launched in 2006. This satellite plays a crucial role in providing a three-dimensional view of clouds and aerosols on a global scale, with observations made every 16 days. One of its main tools, the Cloud-Aerosol Lidar with Orthogonal Polarization (CALIOP), uses a 1,064 nm wavelength channel and two polarization channels at 532 nm. It can effectively capture backscattering information about clouds and aerosols across latitudes ranging from 82° north to south. CALIOP enhances the accuracy of vertical distributions of clouds and aerosols by analyzing backscatter data collected at various atmospheric levels. Notably, as an active remote sensing instrument, CALIOP functions effectively both day and night, independent of the Earth's surface conditions and without the reliance on short-wave solar radiation that characterizes passive remote sensing techniques. As a result, CALIPSO provides a robust and comprehensive dataset for studying the vertical structure and transmission of aerosols in the atmosphere. The collected data included the CALIPSO Level 2 aerosol extinction profiles generated from LIDAR measurements, including aerosol extinction coefficients at various vertical levels. These profiles offer valued insights into the spatial distribution and vertical structure of aerosols within the study area. By analyzing the vertical aerosol extinction profiles obtained from CALIPSO, we are able to characterize the vertical distribution of aerosols and investigate their variability over time.

OMI

The Ozone Monitoring Instrument (OMI) is an important satellite-based sensor that is part of NASA's Aura satellite, launched in 2004. OMI is designed to monitor and collect data on atmospheric composition, particularly ozone and other trace gases. For the data collection of the aerosol Single Scattering Albedo (SSA), we obtained time series data from the OMI (Ozone Monitoring Instrument) satellite sensor. The dataset titled "Time Series, Area-Averaged of SSA 500 nm daily 1 deg." provides daily measurements of SSA at a wavelength of 500 nm, averaged over a spatial resolution of 1 degree. The OMI instrument captures information about aerosol properties in the Earth's atmosphere, including their ability to scatter light, which is quantified by the single scattering albedo. By utilizing this dataset, we aimed to analyze the temporal variations and spatial distribution of SSA over the study area.

Merra-2 Reanalysis

By utilizing the dataset, we aimed to examine the temporal variability and spatial distribution of dust surface mass concentration in the study area. For the dust column mass concentration/density, we utilized data from the MERRA-2 Reanalysis dataset. The dataset titled "Time Series, Area-Averaged of Dust Column Mass Density monthly 0.5 × 0.625 deg." provides monthly measurements of dust column mass density at a spatial resolution of 0.5 × 0.625 degrees. This dataset integrates information about the vertical distribution of dust within the atmosphere, offering an understanding of the total mass of dust particles present in the atmospheric column.

Procedure

The methodology adopted for this study involved several key steps, beginning with the acquisition, preprocessing, and analysis of data related to DEMs and AOD dynamics. The DEM and AOD data were preprocessed to improve quality and eliminate potential inconsistencies, ensuring accurate data for further analysis. First, the DEM data were acquired to characterize the complex topography of the high-altitude region (~4,410 m a.s.l.). The DEM was projected to a common geographic coordinate system to match the spatial reference of the satellite-derived AOD data. Resampling techniques were applied where necessary to harmonize spatial resolution between datasets. Any voids or missing elevation values were filled using interpolation algorithms embedded within the GIS processing software. Slope and elevation layers were derived from the DEM to assess topographic influences on aerosol distribution and atmospheric transport. This step is particularly important in mountainous regions such as Daocheng County, Sichuan, China, where terrain-induced variability can significantly influence aerosol dispersion. Similarly, preprocessing was applied to the aerosol index data obtained from the Sentinel-5P Near Real-Time UV

[2] https://giovanni.gsfc.nasa.gov/giovanni/

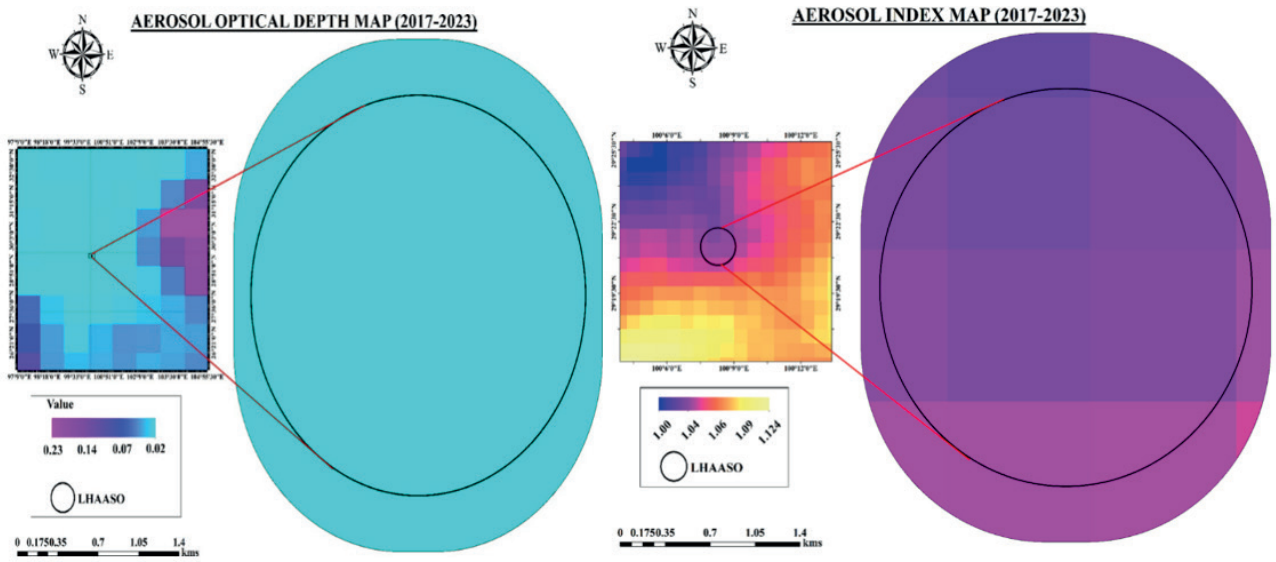

Fig. 3. Mapping of the range of AOD and AI over the LHAASO region from 2017 to 2023

AI dataset. For both the AOD and AI data, pre-processing included: (i) spatial interpolation of all datasets to a common 0.5° × 0.5° grid using bilinear interpolation, which balances computational efficiency with the preservation of spatial gradients; (ii) filtering based on the quality assurance (QA) flags provided by each sensor (e.g., MODIS cloud/surface reflectance flags, Sentinel-5P retrieval confidence flags, and OMI row anomaly filters), thereby excluding low-quality retrievals; and (iii) statistical outlier removal, where values exceeding ±3 standard deviations from the monthly mean were discarded to reduce the influence of spurious satellite retrievals. These steps ensured that only consistent, high-quality data were retained. Importantly, no actual emission sources were removed; instead, the filtering process was designed solely to eliminate data contaminated by cloud interference, snow cover, or algorithm retrieval artifacts.

By following these methodological steps, a robust dataset was compiled, integrating aerosol-related parameters. This comprehensive pre-processing improved the reliability and integrity of the datasets, allowing for an in-depth analysis of the relationship between topography and aerosol dynamics in the study area. CALIPSO vertical profiles were used as an independent constraint to verify the vertical distribution of aerosols, while OMI single scattering albedo was employed to complement MODIS AOD in assessing aerosol radiative properties. No explicit statistical weights were assigned, but each dataset was used in its optimal domain (e.g., MODIS for wide coverage, CALIPSO for vertical profiles), thereby creating a complementary framework.

In addition to descriptive statistics, Pearson correlation was used to evaluate linear relationships, while Spearman rank correlation was employed to capture potential non-linear associations between the study parameters. These statistical tests provide quantitative support for the observed spatial and temporal variability. Statistical tests, including Shapiro–Wilk, Kruskal–Wallis, and Levene's tests, were applied to assess the normality, month-wise variability, and homogeneity of variance of the studied variables. Aerosol vertical profiles were analyzed using linear regression and altitude-based binning to quantify terrain effects on aerosol distribution from 2017 to 2023. Data visualization techniques were employed to create graphs and visual representations, facilitating the interpretation of spatial and temporal trends in AOD and AI values. By following these methodological steps, a robust dataset was compiled, integrating both elevation data and aerosol-related parameters. This integration of multiple data sources, together with systematic pre-processing and cross-validation, ensures a more reliable representation of aerosol dynamics in the study area. The seasonal distribution of AOD is primarily driven by local emissions, boundary-layer dynamics, humidity effects, and wet scavenging during rainfall. Snow cover at higher altitudes may affect retrieval accuracy but does not directly increase AOD. Long-range transport of dust and regional pollution, particularly in the pre-monsoon (Hridoy et al. 2025), also plays a role, while secondary aerosol formation (e.g., sulfate, nitrate) contributes during warmer months. Similar seasonal patterns and drivers have been documented in other high-altitude regions, including the Himalaya, Tibetan Plateau, and observatories such as LHAASO, supporting our interpretation.

RESULTS AND DISCUSSION

Descriptive statistics of monthly variable

The descriptive statistics of the studied monthly variables, namely AOD, AI, and MC are shown in Table 1. The analysis of AOD values across the months reveals significant variations in minimum, maximum, mean, range, standard deviation (SD), coefficient of variation (CV), and skewness. Results demonstrate that January, April, October, and December have the lowest minimum AOD values (0.03, 0.03, 0.00, and 0.03), indicating clearer air, while July records the highest minimum (0.22), reflecting peak aerosol levels. April shows the highest maximum AOD (0.18), with July (0.27) and August (0.21) also reflecting increased aerosols, while November and December have the lowest maximum AOD values (0.04 and 0.05), indicating cleaner air. The mean AOD follows a seasonal trend, with the highest in July (0.24), followed by June (0.17) and August (0.14), and the lowest in November, December, and January (0.03, 0.03, and 0.04), reflecting lower aerosol levels. April shows the highest AOD range (0.15), indicating significant variability, while July shows the smallest range (0.04), indicating more stable conditions. The SD shows the greatest AOD variability in April (0.05), with minimal variation in July (0.02) and December (0.01). The CV highlights extreme variability in October (0.98), while July has the lowest CV (0.07), indicating more stability. Skewness values indicate distribution patterns; April has a strong negative skew (-1.31), suggesting lower AOD values are more frequent. September has strong positive skewness (1.23), indicating higher AOD values are more common. Moderate positive

skewness is observed in July (0.76) and August (0.86), while March (-0.47) and May (-0.34) show negative skewness, indicating lower AOD values. Our results support previous work, which found that using MODIS-based observations recorded a strong association between cloudiness and AOD across many regions of the globe, particularly during the winter and summer seasons (Goto et al. 2019; Singh et al. 2020; Yoon et al. 2012). Overall, AOD levels demonstrate a seasonal trend, with higher concentrations and greater stability in mid-year (June, July, August), particularly in July (mean AOD 0.24), and lower levels with more variability at the start and end of the year (January, November, December), where mean AOD values drop to 0.03-0.04. The AI data demonstrates distinct seasonal variations throughout the year. January shows a minimum AI value of 0.32, while the highest minimum value occurs in August at 1.01, indicating elevated aerosol presence during the late summer. Maximum AI values peak in May at 1.86, reflecting a significant increase in aerosol activity, while the lowest maximum is recorded in January (1.23), suggesting relatively clearer conditions at the year's start. The mean AI values show a steady rise from January (0.68) to May (1.14), with a peak in June (1.19), followed by slightly lower values in July (1.07) and August (1.16). The lowest mean values occur in November (0.81) and December (0.72), reflecting reduced aerosol concentrations at the year's end. The SD is highest in November (0.41), indicating more variability in aerosol levels, while July (0.17) has the lowest SD, reflecting stable conditions. The range of AI values fluctuates, with the largest range in March (1.06) and the smallest in July (0.40), indicating more stable aerosol levels during mid-year. Such varied fluctuation has also been documented in different regions of the continents of Asia and Africa (Wang et al. 2014), and similar findings concur with a 10-Year Record of Aerosol Optical Properties and Radiative Forcing Over Three Environmentally Distinct AERONET Sites in Kenya, East Africa. Specifically, our observed summer AOD peak of 0.27 at LHAASO is comparable to pre-monsoon AOD values reported over the Tibetan Plateau. For instance, Xia et al. (2011) and Liu et al. (2015) reported pre-monsoon AOD values ranging between 0.20 and 0.30 at high-altitude stations on the Plateau, which is consistent with our observations. Similarly, studies over the Andes region (e.g., Segura et al. 2016) have documented seasonal AOD values in the range of 0.18–0.28, highlighting the influence of both local sources and long-range transport in mountainous terrains.

The contribution of different aerosol types to direct radiative forcing over distinct environments of Pakistan inferred from the AERONET data. The CV highlights that November exhibits the highest relative variability (0.51), while July (0.16) shows the lowest, indicating consistency in aerosol presence during mid-year. Skewness values generally indicate a positive skew, with May (1.04) showing the most substantial skewness, suggesting a higher frequency of elevated AI values, while June (0.24) and July (0.23) display the lowest skewness, indicating more balanced distributions of AI levels. Overall, these results show that aerosol activity increases during mid-year with higher stability, while the start and end of the year are characterized by more variability and lower concentrations. The mean MC of particulate matter shows significant seasonal variation across the year. Starting in January, the mean MC is relatively low at 5.83×10^{-6}kg m^{-2}, but it increases gradually through February (12.77×10^{-6} kg m^{-2}) and March (24.12×10^{-6} kg m^{-2}). A peak is observed in April (31.07×10^{-6} kg m^{-2}) and May (26.08×10^{-6} kg m^{-2}), suggesting higher moisture and particulate levels during the mid-year. Following this, a decline in MC is evident, particularly in June (13.51×10^{-6} kg m^{-2}) and July (7.06×10^{-6} kg m^{-2}), reflecting drier conditions. August (6.65×10^{-6} kg m^{-2}) and September (4.14×10^{-6} kg m^{-2}) experience further decreases, reaching their lowest values in September. However, the MC slightly rises again in October (4.80×10^{-6} kg m^{-2}) and November (6.57×10^{-6} kg m^{-2}) before falling to 4.88×10^{-6} kg m^{-2} in December. The range of values is widest in March (22.89×10^{-6} kg m^{-2}) and April (24.50×10^{-6} kg m^{-2}), indicating considerable fluctuation during these months, while the smallest range occurs in December (1.71), suggesting more consistent conditions. The SD also shows greater variability in March, April, and May, with values peaking at 8.14 µg m^{-3} in April. In contrast, the CV reflects a high degree of variability in February (0.37) and November (0.22), with the lowest in December (0.11), suggesting a more stable pattern towards the year's end. The skewness values indicate a generally positive skew, especially in February (0.83) and March (0.43), suggesting a tendency for higher MC values in these months, while a negative skew in December (-0.53) indicates a shift toward lower concentrations. This data reflects a clear seasonal fluctuation in MC, with the highest levels observed during the mid-year, followed by a decrease toward the year-end.

Aerosol Optical Depth

AOD is a measure of how much sunlight is blocked or scattered by particles such as dust, smoke, and pollution in the atmosphere (Akinyoola et al. 2024; Ruiz-Arias et al. 2016). Basically, AOD quantifies the extinction of solar radiation due to aerosol particles, indicating the extent to which direct sunlight is prevented from reaching the Earth's surface (Goto et al. 2019; Singh et al. 2020). The monthly AOD data from 2017 to 2023 were analyzed to assess the temporal variation of AOD in the study area, as shown in Fig. 4. The data reveals noticeable fluctuations in AOD levels throughout the year, across different years. In 2017, for example, AOD values start relatively low in January, gradually increasing to peak levels around March or April before declining toward the end of the year. However, the highest recorded AOD values occurred in June and July, with a subsequent decrease after October. This seasonal pattern is consistent across the following years, although the specific magnitude of AOD values varies slightly from year to year. In recent studies, it was found that AOD performs well in characterizing seasonal differences across the desert and urban/built environments across the world, where the AOD retrievals reveal underestimation in the desert area of Southeast Asia. Besides, the frequent reoccurrences of the dry/hot boundary layer driven by large-scale circulation patterns tend to lead to the AOD underestimation (Stirnberg et al. 2018).

In addition, monthly AOD values demonstrate a degree of consistency across the years, particularly in certain months. For instance, July consistently exhibits higher AOD values compared to other months, suggesting a seasonal trend or environmental factors that influence aerosol concentrations during this period. By analyzing the individual monthly AOD graphs, a detailed examination of AOD dynamics over time can be conducted, revealing significant variations and anomalies. Comparing AOD trends across different years reveals important patterns in long-term trends and seasonal variability of aerosol concentrations within the study area. The average annual AOD values range from approximately 0.097 to 0.120, indicating relatively consistent aerosol concentrations in the atmosphere. However, noticeable fluctuations in the maximum and minimum AOD values reflect the dynamic nature of aerosol distribution and atmospheric conditions. Notably, 2023 shows the highest average AOD value of

Table 1. Descriptive statistics of the studied monthly variables, namely, AOD, AI, and MC (10^{-6} kg m^{-2})

		Jan	Feb	Mar	Apr	May	Jun	Jul	Aug	Sep	Oct	Nov	Dec
AOD	Min	0.03	0.05	0.11	0.03	0.05	0.13	0.22	0.11	0.11	0.00	0.03	0.03
	Max	0.06	0.10	0.17	0.18	0.13	0.19	0.27	0.21	0.15	0.07	0.04	0.05
	Range	0.03	0.05	0.06	0.15	0.08	0.07	0.04	0.10	0.04	0.06	0.01	0.02
	Mean	0.04	0.07	0.14	0.14	0.10	0.17	0.24	0.14	0.12	0.03	0.03	0.03
	SD	0.01	0.02	0.02	0.05	0.03	0.03	0.02	0.04	0.02	0.03	0.01	0.01
	CV	0.24	0.24	0.14	0.35	0.27	0.16	0.07	0.28	0.14	0.98	0.17	0.20
	Skewness	0.56	0.41	-0.47	-1.31	-0.34	-0.31	0.76	0.86	1.23	0.26	0.25	0.65
AI	Min	0.32	0.44	0.49	0.63	0.83	0.80	0.89	1.01	0.96	0.71	0.31	0.37
	Max	1.23	1.39	1.56	1.45	1.86	1.58	1.29	1.54	1.71	1.51	1.43	1.25
	Range	0.91	0.96	1.06	0.82	1.03	0.78	0.40	0.53	0.75	0.79	1.12	0.89
	Mean	0.68	0.80	0.89	0.95	1.14	1.19	1.07	1.16	1.26	1.07	0.81	0.72
	SD	0.31	0.35	0.37	0.31	0.35	0.29	0.17	0.20	0.26	0.30	0.41	0.33
	CV	0.45	0.44	0.41	0.33	0.31	0.25	0.16	0.17	0.21	0.28	0.51	0.45
	Skewness	0.61	0.56	0.67	0.55	1.04	0.24	0.23	0.96	0.45	0.38	0.36	0.57
MC	Min	4.49	7.95	14.43	18.46	18.43	8.02	3.92	4.34	3.28	3.94	5.22	3.88
	Max	8.32	22.04	37.32	42.97	34.46	19.13	10.68	10.49	5.21	7.19	9.21	5.60
	Range	3.83	14.09	22.89	24.50	16.04	11.11	6.76	6.15	1.93	3.24	3.99	1.71
	Mean	5.83	12.77	24.12	31.07	26.08	13.51	7.06	6.65	4.14	4.80	6.57	4.88
	SD	1.29	4.73	7.45	8.14	5.91	4.01	2.39	2.25	0.67	1.08	1.48	0.55
	CV	0.22	0.37	0.31	0.26	0.23	0.30	0.34	0.34	0.16	0.22	0.22	0.11
	Skewness	0.83	0.83	0.43	0.01	-0.02	0.07	0.21	0.51	0.26	1.47	0.67	-0.53

Note: Descriptive statistics of the studied monthly variables, namely AOD, AI, and MC, derived from combined satellite observations (MODIS, Sentinel-5P) and reanalysis datasets (MERRA-2). The table summarizes the mean, SD, minimum (Min), maximum (Max), and range, coefficient of variation (CV), and skewness for each variable.

0.12, along with a peak AOD value of 0.27. This suggests a potential increase in aerosol loading during that year, highlighting the need for further investigation into the factors contributing to this rise. Our results support the findings of previous studies conducted across many parts of the region. More than 30 critical fields concentrated on and directed across North America, Europe, and China have researched the science of tropospheric ozone, meteorological examples, forerunner emanations, and displaying endeavors (Solomon et al. 2000). Moreover, research on black carbon has zeroed in on BC and PM10 levels, close by air contamination files, in the locales of Beijing and Lhasa between January and December 2006 (Gao et al. 2007).

The year 2018 stands out with the lowest minimum AOD value of 0.003, indicating relatively clear atmospheric conditions during that period. Such variations in AOD extremes highlight the significance of closely monitoring aerosol dynamics to assess air quality and their broader environmental impacts. The annual summary of AOD trends provides essential insights into the temporal variability of aerosol concentrations in the study area, setting the stage for further analysis and interpretation in the subsequent sections. Distinct patterns in AOD levels emerge across the months, with periods like July showing higher average AOD values, suggesting elevated aerosol concentrations during this season. Conversely, months like October demonstrate lower average AOD values, indicating cleaner atmospheric conditions. Recognizing these seasonal fluctuations in AOD is critical for understanding air quality environmental impacts and informing effective mitigation strategies.

Aerosol Index

The AI is a qualitative measure indicating the presence of elevated aerosol layers with significant absorption, primarily from desert dust, biomass burning, and volcanic ash plumes. Analyzing monthly AI data from 2017 to 2023 presented in Fig. 5 reveals substantial variations in aerosol concentrations throughout the year, with peak values typically observed in the summer months of May, June, and July and lower values in winter, particularly January and February. Inter-annual variability is also notable, with the year 2020 exhibiting elevated AI values across several months. From 2017 to 2023, the annual average mean AI values range from 0.730 to 1.330, reflecting the average aerosol loading in the atmosphere each year. Seasonal changes, regional air pollution, and meteorological conditions can influence variations in these values. Notably, 2020 recorded the highest annual average AI

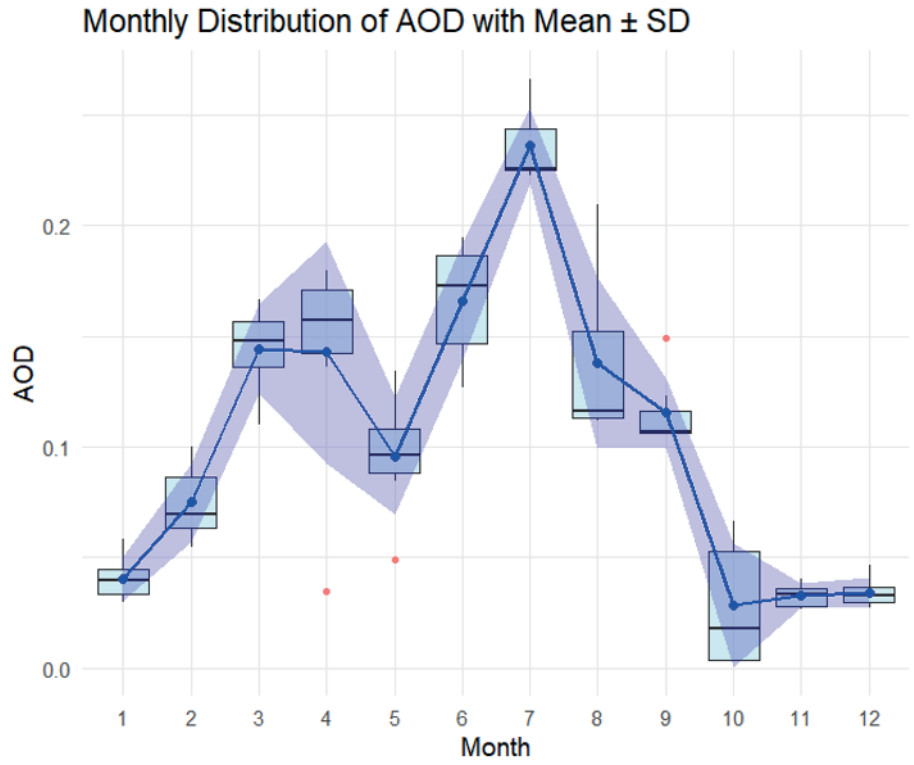

Fig. 4. Mean monthly distribution of AOD. The light blue boxplots represent the full monthly range, including outliers (red points), while the blue line and points indicate the monthly mean. The shaded blue area around the mean represents SD, highlighting the variability within each month

value of 1.330, suggesting elevated aerosol concentrations, possibly linked to increased anthropogenic activities or environmental events. Maximum AI values, which indicate the peak aerosol concentrations within a year, ranged from 1.028 to 1.855. The year 2019 had the highest maximum AI value of 1.474, marking a significant aerosol event. Minimum AI values ranged from 0.315 to 0.940, with 2022 showing the lowest minimum AI of 0.315, indicating a period of relatively cleaner air. The aerosol distributions during the interannual variability and seasonal changes could be attributed to winter large fractions of the Asian dust and Indian Ocean with a strong correlation with the physical atmospheric mechanism (Das Mahapatra et al. 2022; Gandham et al. 2022; Jin et al. 2021). However, such associated controlling phenomena can be attributed to dust emission from the dryland of the region, which is in agreement with previous studies (Duniway et al. 2019; Huang et al. 2017).

The calculated mean AI values across the months from January to December reveal distinct seasonal patterns. The winter months of January and February show lower mean AI values, ranging from 0.679 to 0.799, likely due to reduced biological and anthropogenic aerosol emissions and stable atmospheric conditions. In the spring, mean AI values gradually increase to a range of 0.888 to 1.138, driven by factors such as increased vegetation activity, dust storms, and biomass-burning events. Summer months, from June to August, see higher mean AI values, ranging from 1.138 to 1.187, which can be attributed to increased atmospheric instability, higher temperatures, and intensified human activity. During autumn, mean AI values remain elevated, ranging from 1.067 to 1.257, influenced by agricultural practices, regional wildfires, and atmospheric circulation patterns. In December, mean AI values slightly decrease to a range of 0.724 to 0.805, reflecting lower biomass burning and reduced anthropogenic emissions as temperatures drop and seasonal activities change.

Aerosol Extinction Coefficient

The results of aerosol extinction coefficients at various altitudes from 2017 to 2023 indicate fluctuations in aerosol concentration and distribution within the atmosphere over the study period. At lower altitudes, ranging from 1 km to 3 km, the aerosol extinction coefficients exhibit relatively low values, typically below 0.01 km-1. However, there are sporadic increases observed in certain years, particularly in 2020 and 2023, where slightly elevated values are noted, possibly attributed to localized aerosol events or meteorological conditions influencing aerosol transport and dispersion.

Moving to higher altitudes, between 4 and 7 km, the aerosol extinction coefficients show more pronounced variability across the years. Multiple time series extinction coefficients at various altitudes from 2017 to 2023 are seen in Fig. 6. In some instances, such as at 5 km altitude, significant increases in aerosol extinction coefficients are observed, notably in 2017 and 2019, suggesting the presence of elevated aerosol layers or enhanced atmospheric aerosol loading during those periods. Conversely, there are instances of decreased aerosol extinction coefficients in certain years, indicating temporal variability in aerosol distribution and concentration profiles within the mid-tropospheric region. At altitudes exceeding 7 km, aerosol extinction coefficients generally remain relatively low, with occasional minor fluctuations observed across the years. However, it's worth noting the substantial increase in aerosol extinction coefficients observed at 6 km altitude in 2018, primarily attributed to localized aerosol events or transient atmospheric phenomena impacting aerosol concentrations at that altitude level. The results highlight the dynamic aerosol distribution and concentration profiles driven by atmospheric dynamics, meteorological conditions, and aerosol emission sources.

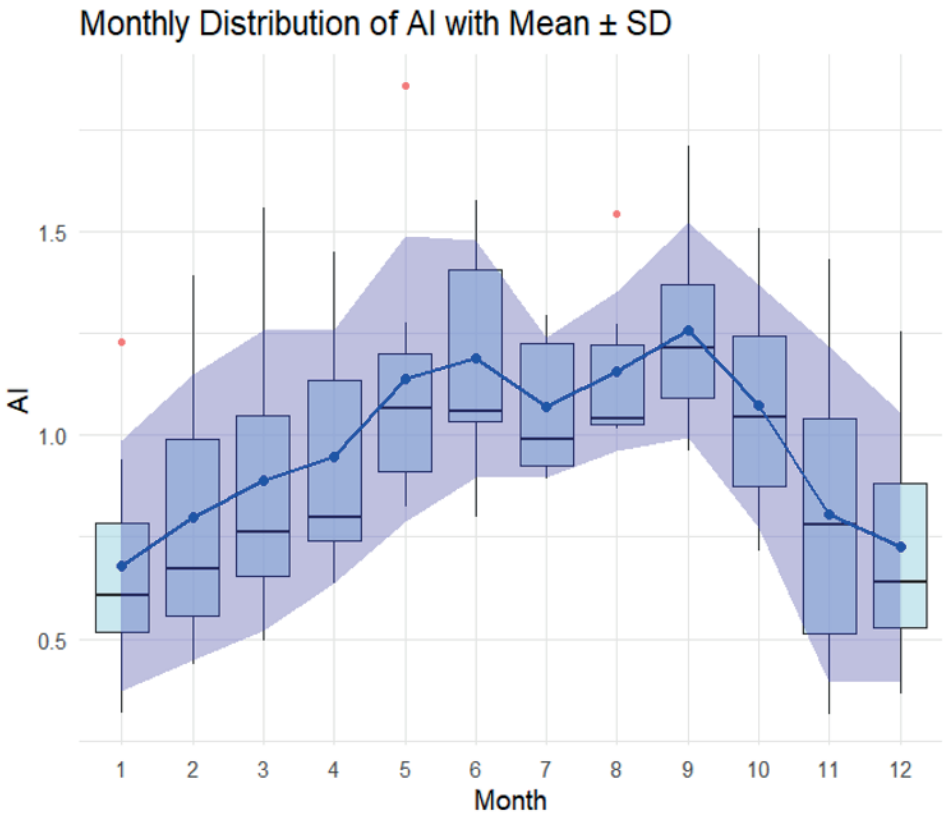

Fig. 5. Mean monthly distribution of AI. The light blue boxplots represent the full monthly range, including outliers (red points), while the blue line and points indicate the monthly mean. The shaded blue area around the mean represents SD, highlighting the variability within each month

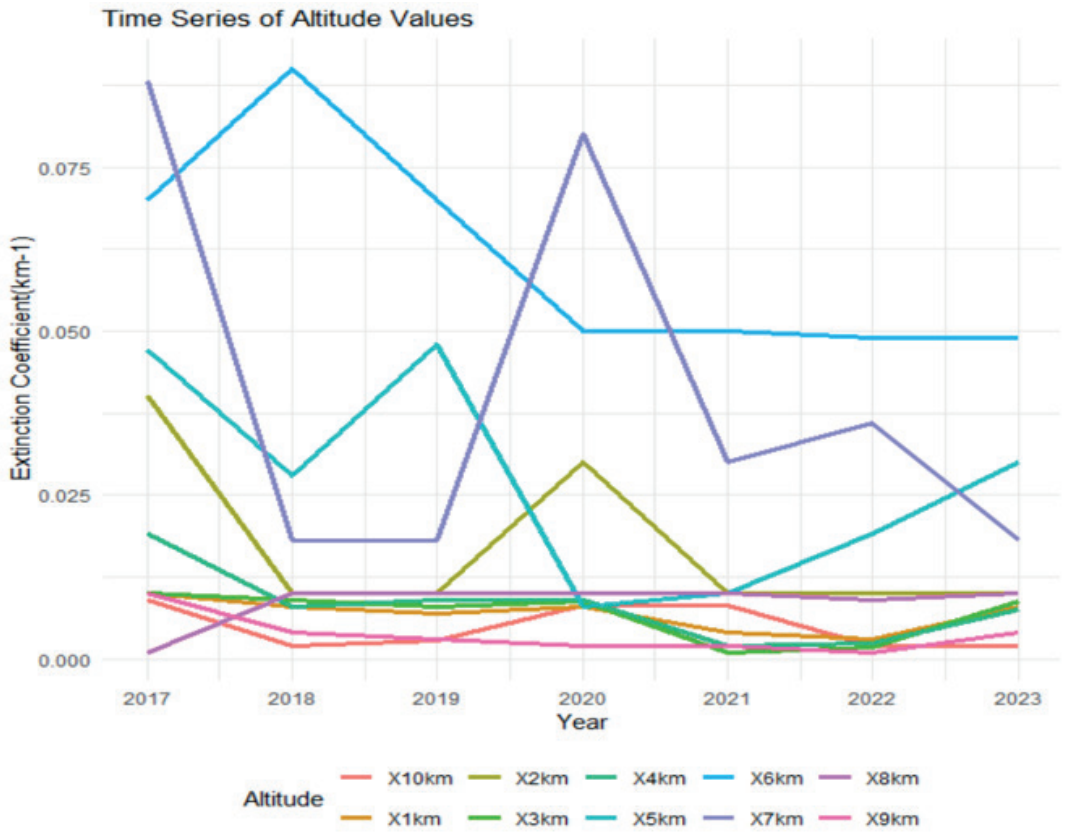

Fig. 6. Multiple time series extinction coefficients at various altitudes from 2017 to 2023

Mass concentration & Single scattering albedo

For the study period, the aerosol mass concentration exhibits notable fluctuations, indicative of changes in aerosol emissions, atmospheric transport, and deposition processes. In 2018, a significant increase in aerosol concentration was observed, with a value of 15.15 kg m^{-2} 10^{-6}, representing a peak in aerosol loading during the analyzed years. The increase in aerosol concentration indicates either stronger emissions or greater atmospheric transport of particles, likely driven by regional sources, meteorological factors, or human activities.

Conversely, a decline in aerosol concentration was noted in 2020, with a value of 9.49 kg m^{-2} 10^{-6}, representing

a notable reduction compared to preceding years. On the other hand, the monthly averaged plot did not show a significant increase between 1980 and 2018. Along the North African coast, the values range from 0.24×10^{-6} kg m^{-2} month^{-1} (eastern Egypt) to 0.63×10^{-6} kg m^{-2} month^{-1} (southern Tunisia), while in marine areas, they vary from 0.26×10^{-6} kg m^{-2} month^{-1} (Balearic Islands) to 0.48×10^{-6} kg m^{-2} month^{-1} (Malta) (Bibi et al. 2020). This decrease in aerosol concentration may be attributed to changes in emissions patterns, atmospheric circulation patterns, or meteorological conditions leading to reduced aerosol transport and deposition within the study area. The monthly patterns of mass concentration and single scattering albedo over the LHAASO from 2017- 2023 are presented in Fig. 7. The subsequent years, 2021 to 2023, witnessed a moderate increase in aerosol concentration compared to 2020 but remained lower than the peak observed in 2018. These fluctuations in aerosol concentration highlight the complex interplay of various factors influencing aerosol dynamics, including emission sources, atmospheric circulation patterns, precipitation events, and atmospheric stability. Overall, the temporal variability in aerosol concentration underscores the dynamic nature of aerosol processes within the study area and emphasizes the importance of continuous monitoring and analysis to better understand the drivers and implications of aerosol variability on atmospheric composition, air quality, and climate dynamics (Li et al. 2024; Perumpully & Gautam 2024).

The analysis of SSA revealed consistent patterns across the study period from 2017 to 2023. The SSA values ranged from approximately 0.935 to 0.942, indicating the fraction of light scattered by aerosol particles relative to their total extinction. Over the years, there was a slight downward trend in the SSA values, with a gradual decrease observed from 2017 to 2023. This decline suggests potential changes in the composition or optical properties of aerosol particles in the atmosphere. Factors such as variations in aerosol sources, transport mechanisms, and atmospheric conditions could contribute to these temporal trends in SSA. The relatively stable SSA values across the study period indicate consistent aerosol scattering characteristics within the region. However, the observed decline over time may reflect shifts in aerosol composition or size distribution, which can influence their scattering properties (Kaufman et al. 1994). The results obtained in the present studies are similar to those of Pakistan using clustering techniques between different major cities of Pakistan, identifying distinct classifications of aerosol over the region.

Dust surface and Column density

The dust surface density, representing the mass of dust per unit area at the Earth's surface, exhibited a relatively stable pattern across the years, with values ranging from approximately 1.1×10^{-11} to 1.5×10^{-11} kg m^{-2}. Similarly, the dust column density, which indicates the total mass of dust per unit area within a vertical column of the atmosphere, displayed consistent values ranging from approximately 2.8×10^{-5} to 4.5×10^{-5} kg m^{-2}. The monthly patterns of dust column density are presented in Fig. 8. The temporal stability observed in both dust surface and column mass concentrations suggests a relatively constant presence of airborne dust particles in the atmosphere over the study period. Besides, high groupings of residue particles can lead to respiratory issues and increment non-inadvertent mortality (Pu & Ginoux 2018). However, minor fluctuations in dust density values from year to year may reflect variations in dust emission sources, atmospheric circulation patterns, and meteorological conditions. Factors such as wind speed, land surface properties, and regional climate dynamics can influence the generation, transport, and deposition of dust particles, contributing to the observed variations in dust mass concentrations. On the other hand, it has been observed that the long-term dust concentration measured over a specific region is attributed to weak correlations between the North Atlantic Oscillation and surface concentration during the winter season (Ginoux et al. 2004). Thus, such extended imitation highlights key information to explore the North Atlantic Oscillation effects on dust distribution rather than limited and/or affected regions at the edge of that phenomenon (Tao et al. 2017; Wang et al. 2007; Xie et al. 2011; Yang et al. 2022).

Correlation analysis and statistical evaluation of the studied variables

The Pearson and Spearman correlation analyses revealed distinct relationships between aerosol and studied variables from 2017 to 2023 (Fig. 9). For Pearson correlations, AOD exhibited moderate positive associations with SSA (r = 0.571), AI (r = 0.292), dust column density (r = 0.274), and

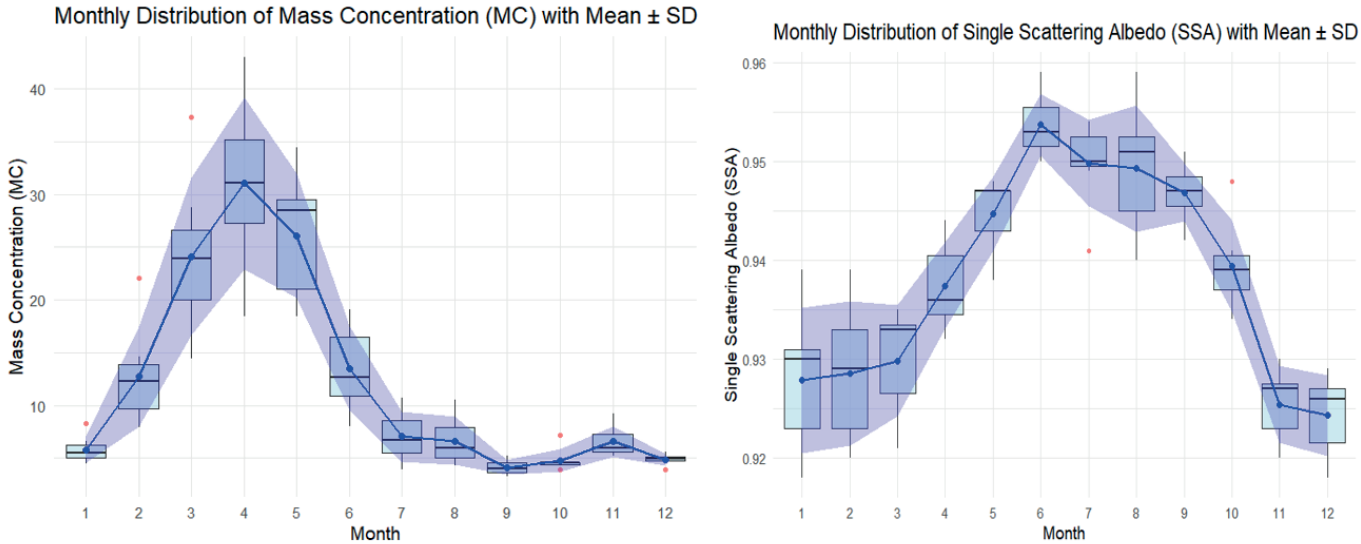

Fig. 7. Mean monthly distribution of MC (kg m^{-2} 10^{-6}) and SSA. The light blue boxplots represent the full monthly range, including outliers (red points), while the blue line and points indicate the monthly mean. The shaded blue area around the mean represents SD, highlighting the variability within each month

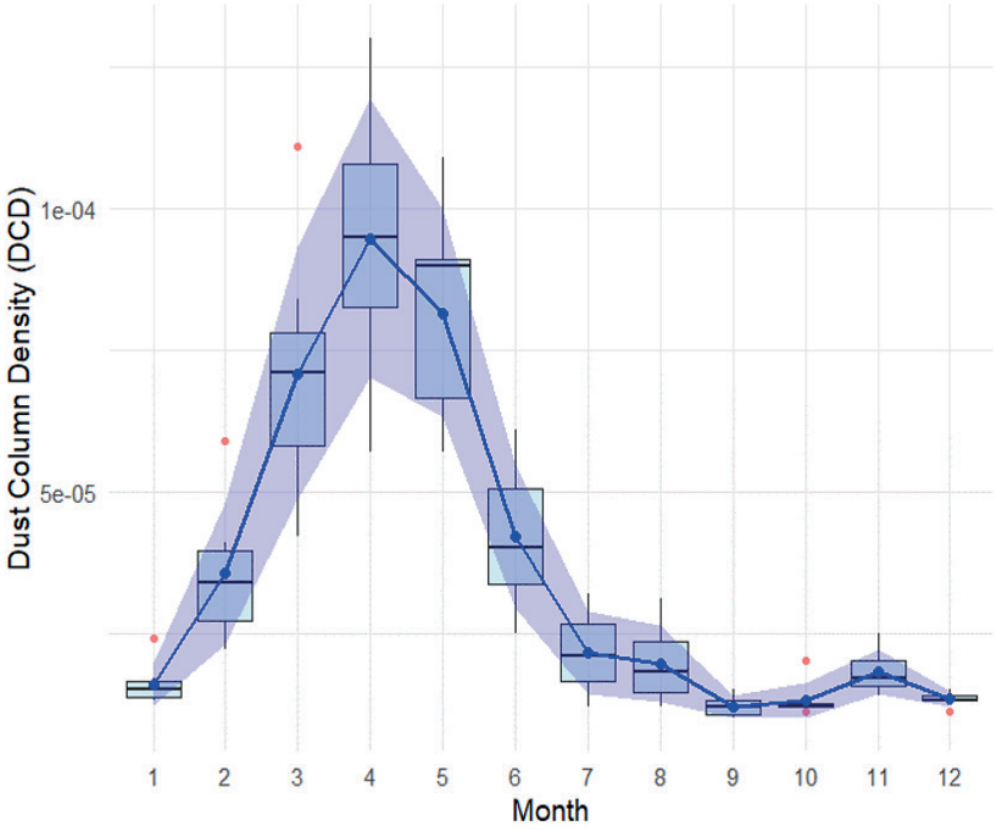

Fig. 8. Mean monthly distribution of dust column density (kg m^{-2}). The light blue boxplots represent the full monthly range, including outliers (red points), while the blue line and points indicate the monthly mean. The shaded blue area around the mean represents SD, highlighting the variability within each month

MC (r = 0.258), suggesting that higher AOD coincides with higher aerosol scattering efficiency and slightly increased mass and columnar dust. AI showed a moderate positive correlation with SSA (r = 0.399) but negligible correlations with MC (r = –0.028) and DCD (r = –0.011), indicating limited linear association between atmospheric aerosol presence and dust quantities. As expected, MC and dust column density were strongly correlated (r = 0.998), reflecting the nearly identical patterns of dust mass and column density in the study area. SSA displayed very weak correlations with MC (r = 0.001) and DCD (r = 0.034), indicating that aerosol scattering properties are largely independent of absolute dust concentrations.

Spearman rank correlations, which capture monotonic relationships, were largely consistent with the Pearson results but slightly stronger for some variables. AOD correlated positively with SSA (ρ = 0.593), MC (ρ = 0.354), dust column density (ρ = 0.394), and AI (ρ = 0.313), reflecting consistent rank-order associations. AI again showed a moderate positive correlation with SSA (ρ = 0.409) but weak negative correlations with MC (ρ = –0.090) and DCD (ρ = –0.069). The MC– dust column density relationship remained extremely strong (ρ = 0.995), confirming their near-identical monotonic behavior. SSA correlations with MC (ρ = 0.006) and DCD (ρ = 0.054) remained negligible, reinforcing that aerosol scattering efficiency is not closely associated with dust mass or column density. Overall, these results suggest that AOD and SSA are moderately related, whereas dust quantity variables (MC and dust column density) are strongly interrelated but largely independent of aerosol scattering properties.

Statistical tests were conducted to assess the variability and distribution characteristics of aerosol and dust-related variables from 2017 to 2023 as shown in Table 2. The Shapiro–Wilk test indicated that AI was normally distributed (p = 0.508), whereas AOD (p = 0.0017), dust column density (p < 0.001), MC (p < 0.001), and SSA (p = 0.0121) significantly deviated from normality, suggesting non-parametric methods were appropriate for further analysis. The Kruskal–Wallis test, examining month-wise variability, revealed that all variables except AI exhibited significant differences across months, with AOD, dust column density, MC, and SSA all showing p-values < 0.001, while AI demonstrated moderate variability (p = 0.0107). This confirms that aerosol optical depth, dust mass, dust column density, and scattering properties exhibit strong temporal variability on a monthly scale. Levene's test for homogeneity of variance showed that AI (p = 0.969), AOD (p = 0.330), and SSA (p = 0.685) had relatively stable variances across months, whereas dust column density (p = 0.0003) and MC (p = 0.0006) displayed significant heterogeneity, reflecting greater fluctuations in dust quantities compared to optical properties. Results indicate that AOD, dust column density, MC, and SSA significantly deviate from normality and exhibit substantial monthly variability, whereas AI shows moderate variability and homogenous variance. Collectively, these results provide robust statistical evidence that aerosol and dust characteristics vary significantly over time, with dust mass and column density exhibiting the most pronounced variability, while aerosol optical properties such as AI and SSA are comparatively more stable.

Relationship between aerosol extinction coefficient (EC) and terrain

A linear regression analysis was performed to assess the relationship between EC values and altitude from 1 to 10 km over the period 2017–2023 (Fig. 10) The regression model yielded an intercept of 0.0175 (±0.0057, p = 0.00298), indicating the expected EC value at sea level. The slope for altitude was 0.000185 ± 0.000917 (p = 0.841), suggesting a very weak and statistically non-significant increase in the

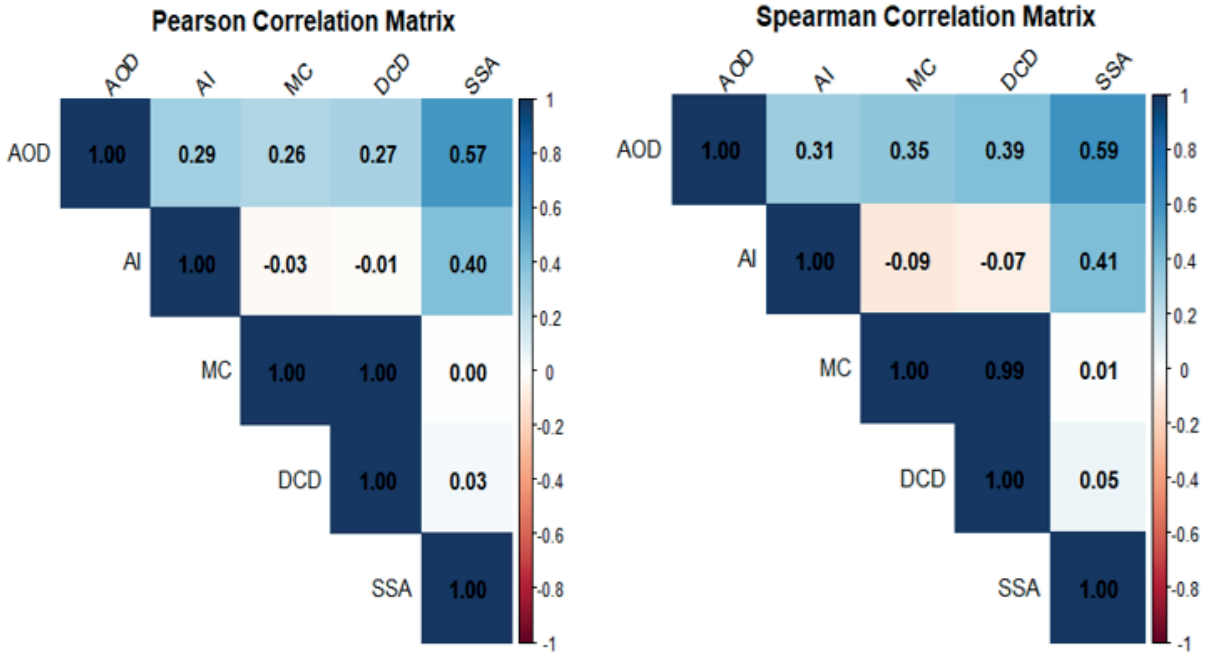

Fig. 9. Matrices showing pairwise correlations among aerosol and studied variables from 2017 to 2023. (a) Pearson correlation matrix, illustrating linear relationships between AOD, AI, MC, dust column density (DCD), and SSA. (b) Spearman rank correlation matrix, capturing monotonic associations between the same variables

Table 2. Summary of statistical tests for aerosol and dust-related variables from 2017 to 2023. Shapiro–Wilk test assesses the normality of each variable, with p < 0.05 indicating deviation from normality. Kruskal–Wallis test evaluates significant month-wise differences in variable values, with p < 0.05 indicating significant variability. Levene's test examines homogeneity of variance across months, with p < 0.05 indicating heterogeneity

Variable	Shapiro-Wilk test	Kruskal-Wallis test	Levene's test
AI	0.5078	0.01070	0.96910
AOD	0.0017	0.00000	0.32980
Dust column density	0.0000	0.00000	0.00030
MC	0.0000	0.00000	0.00060
SSA	0.0121	0.00000	0.68500

values with increasing altitude. The residuals ranged from –0.0182 to 0.0714, with a median of –0.0090, reflecting minor deviations from the fitted line. The model explained only a negligible fraction of the variance in EC values, with a multiple R-squared of 0.0006 and an adjusted R-squared of –0.0141. The F-statistic was 0.041 (p = 0.841), confirming that altitude does not significantly predict aerosol concentrations in this dataset. These results indicate that, over the study region, EC values are largely independent of altitude, and any terrain-related effects on vertical aerosol distribution are minimal within the observed altitude range.

The aerosol extinction coefficient values were further analyzed by stratifying the data into 2 km altitude bins to examine potential terrain effects (Fig. 11). The mean EC value in the lowest altitude bin (0–2 km) was 0.012 with a standard deviation of 0.0102 (n = 14), indicating relatively low and moderately variable concentrations. In the 2–4 km bin, the mean decreased to 0.00743 with a standard deviation of 0.00464 (n = 14), reflecting the lowest aerosol concentrations observed across all bins. Extinction coefficient values increased substantially in the 4–6 km bin, with a mean of 0.0441 and a standard deviation of 0.0234 (n = 14), representing the highest concentrations and greater variability, suggesting localized accumulation at mid-altitudes. The 6–8 km bin exhibited a mean EC value of 0.0249 with a higher standard deviation of 0.0267 (n = 14), indicating considerable temporal variability at these altitudes. Finally, the 8–10 km bin had the lowest mean EC value of 0.0043 with a standard deviation of 0.00312 (n = 14), highlighting minimal aerosol presence at higher altitudes. Overall, the stratified analysis demonstrates that aerosol concentrations peak at mid-altitudes (4–6 km) and decrease toward both lower and higher altitudes, with variability generally increasing at intermediate altitudes, suggesting that terrain and atmospheric processes may influence vertical aerosol distribution.

CONCLUSION

Seven years of satellite-based observations over LHAASO from 2017 to 2023 were used to analyze aerosol optical features AOD, AI, SSA, EC, MC, and dust surface and column density. This study concludes that peak AOD levels typically occur in the spring and summer when dust transport and biomass burning are most prevalent. AI values showed significant seasonal variation. SSA values suggest that aerosols were predominantly scattering in nature, with some absorption components. EC reflects variations in aerosol loading and composition over time. Mass concentration values also exhibited seasonal shifts, particularly during the dust season when higher concentrations were recorded, compared to lower concentrations during non-dust periods. Column densities

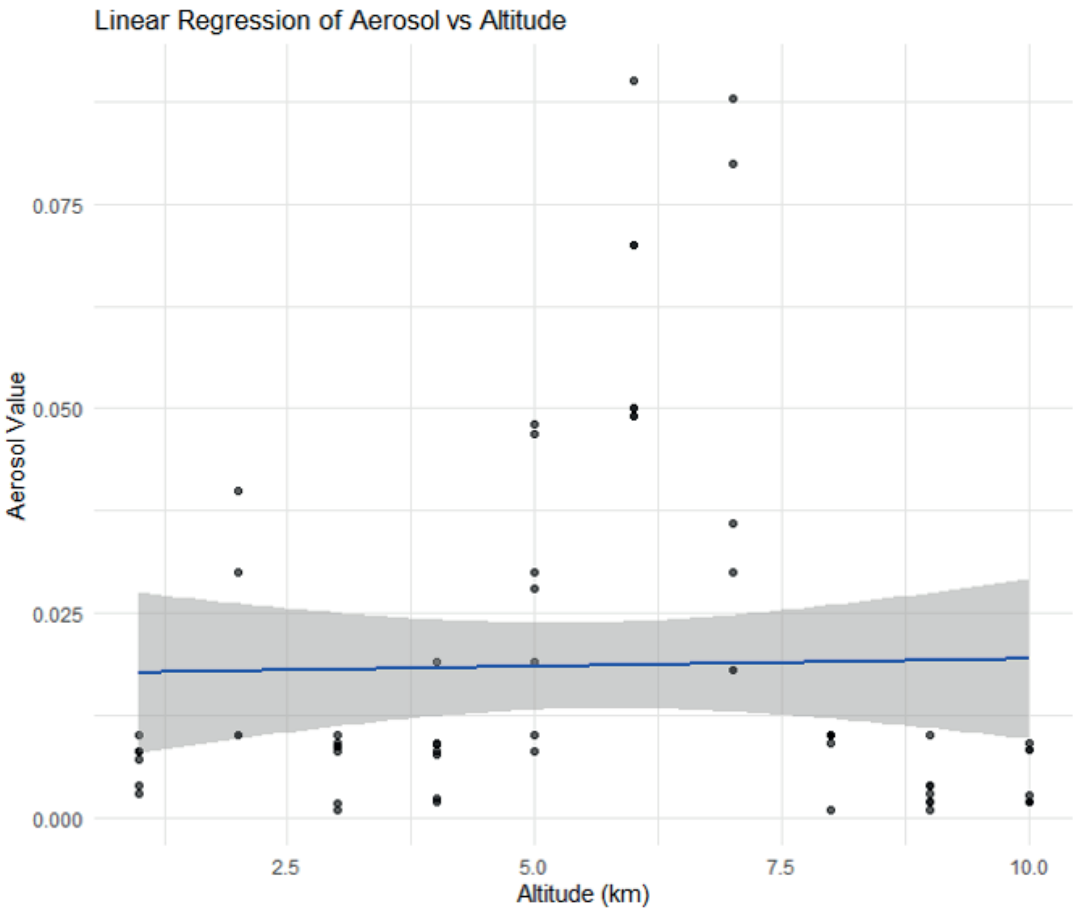

Fig. 10. Linear regression of aerosol extinction coefficient values against altitude (1–10 km) from 2017 to 2023. The regression line (blue) with a 95% confidence interval shows a non-significant relationship (slope = 0.000185, p = 0.841), indicating that aerosol concentrations are largely independent of altitude in the study region

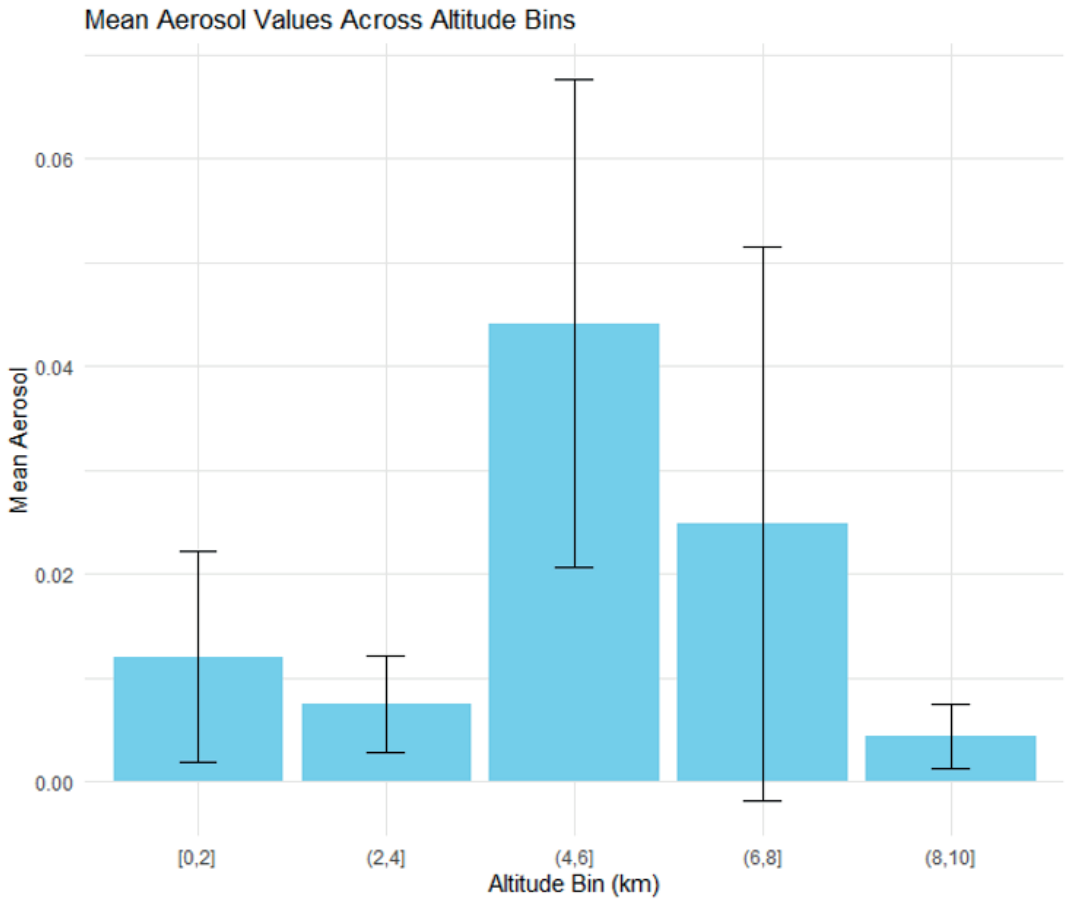

Fig. 11. Mean extinction coefficient values and standard deviations across 2 km altitude bins from 0 to 10 km over the period 2017–2023. Aerosol concentrations peak at mid-altitudes (4–6 km) and are lowest at both lower and higher altitudes, highlighting potential influences of terrain and atmospheric processes on vertical aerosol distribution

showed an increase of up to 30% during dust transport events, illustrating the influence of desert sources on local aerosol composition. These results enhance our understanding of local aerosol characteristics over LHAASO and their climatic implications, and they provide a basis for future improvements in regional climate modeling and air-quality assessments.

REFERENCES

Akinyoola, J. A., Oluleye, A., & Gbode, I. E. (2024). A Review of Atmospheric Aerosol Impacts on Regional Extreme Weather and Climate Events. Aerosol Science and Engineering, 8(3), 249-274.

Andrews E, Ogren JA, Bonasoni P, Marinoni A, Cuevas E, Rodríguez S et al (2011) Climatology of aerosol radiative properties in the free troposphere. Atmos Res 102(4): 365–393.

Bhowmik, R. C., Islam, S., Roy, S. K., Hridoy, M. A. A. M., Yeamin, M. B., Hoque, M. A., ... & Roshid, M. M. (2025). The Role of Hydropower, Clean Energy, Renewable Energy, FDI, and Capital Formation in Affecting CO2 Emissions and Environmental Sustainability in South Asia. Environment, Innovation and Management, 1, 2550021.

Bibi, H., Alam, K., & Bibi, S. (2016). In-depth discrimination of aerosol types using multiple clustering techniques over four locations in Indo-Gangetic plains. Atmospheric Research, 181, 106-114.

Bibi, M., Saad, M., Masmoudi, M., Laurent, B., & Alfaro, S. C. (2020). Long-term (1980–2018) spatial and temporal variability of the atmospheric dust load and deposition fluxes along the North-African coast of the Mediterranean Sea. Atmospheric Research, 234, 104689.

Bilal M et al (2019) Evaluation of Terra-MODIS C6 and C6.1 aerosol products against Beijing, XiangHe, and Xinglong AERONET Sites in China during 2004–2014. Remote Sens 11:486

Blaga, R., & Gautam, S. (2024). Improving PM10 sensor accuracy in urban areas through calibration in Timişoara. NPJ Climate and Atmospheric Science, 7(1), 268.

Boucher O, Randall D, Artaxo P, Bretherton C, Feingold G, Forster P et al (2013) Clouds and aerosols. In: Climate change 2013: the physical science basis. Contribution of Working Group I to the Fifth Assessment Report of the Intergovernmental Panel on Climate Change. Cambridge University Press, p 571–657.

Das Mahapatra, P., Abhilash, S., & Ruchith, R. D. (2022). Aerosol distribution during spring and summer and its relationship with Inter-Annual variability of summer monsoon rainfall over Indian region. Geocarto International, 37(26), 11441-11455.

Delene DJ, Ogren JA (2002) Variability of aerosol optical properties at four North American surface monitoring sites. J Atmos Sci 59(6):1135–1150.

Duniway, M. C., Pfennigwerth, A. A., Fick, S. E., Nauman, T. W., Belnap, J., & Barger, N. N. (2019). Wind erosion and dust from US drylands: a review of causes, consequences, and solutions in a changing world. Ecosphere, 10(3), e02650.

Edenhofer O, Seyboth K (2013) Intergovernmental panel on climate change (IPCC).

Gautam S, Gautam AS, Singh K, James EJ, Brema J (2021) Investigations on the relationship among lightning, aerosol concentration, and meteorological parameters with specific reference to the wet and hot humid tropical zone of the southern parts of India. Environ Technol Innov. https:// doi. org/ 10. 1016/j. eti. 2021. 101414.

Gautam, S., Blessy, A., Abhilash, P., Yadav, A., & Justin, A. (2024). Exploring radiative forcing sensitivity to aerosol optical properties across varied geographical regions in India. Air Quality, Atmosphere & Health, 17(8), 1689-1700

Gandham, H., Dasari, H. P., Karumuri, A., Ravuri, P. M. K., & Hoteit, I. (2022). Three-dimensional structure and transport pathways of dust aerosols over West Asia. npj Climate and Atmospheric Science, 5(1), 45.

Gao, R., Niu, S., Zhang, H., Guo, J., Meng, D., Ma, J., ... & Zhang, Y. (2007, October). A comparative study on black carbon aerosol observations in regions of Beijing and Lhasa in 2006. In Remote Sensing and Modeling of Ecosystems for Sustainability IV (Vol. 6679, pp. 533-540).

Ginoux, P., Prospero, J. M., Torres, O., & Chin, M. (2004). Long-term simulation of global dust distribution with the GOCART model: correlation with North Atlantic Oscillation. Environmental Modelling & Software, 19(2), 113-128.

Gong W, Zhang M, Han G, Ma X, Zhu Z (2015) An investigation of aerosol scattering and absorption properties in Wuhan, Central China. Atmosphere 6:503–520.

Goto, D., Kikuchi, M., Suzuki, K., Hayasaki, M., Yoshida, M., Nagao, T. M., ... & Nakajima, T. (2019). Aerosol model evaluation using two geostationary satellites over East Asia in May 2016. Atmospheric Research, 217, 93-113.

Hridoy, M. A. A. M., & Paul, P. B. (2024). Assessing Total Dissolved Oxygen and Electrical Conductivity Using Sentinel-2 Remote Sensing: A Multivariable Approach to Flood Detection in Flood-Prone Urban area Sylhet.

Hridoy, M. A. A. M., Akter, P., Bordin, C., Acharjee, M. R., Baki, A. O., Neogi, S., ... & David, G. S. (2025). Integrated Assessment of Heavy Metal Contamination and Human Health Risks in Granitic Soils of South India: A Multi-Index Approach to Pollution and Ecological Impacts. Results in Surfaces and Interfaces, 100628.

Hridoy, M. A. A. M., Bordin, C., Masood, A., & Masood, K. (2025). Predictive modelling of aquaculture water quality using IoT and advanced machine learning algorithms. Results in Chemistry, 16, 102456.

Huang, J., Li, Y., Fu, C., Chen, F., Fu, Q., Dai, A., ... & Wang, G. (2017). Dryland climate change: Recent progress and challenges. Reviews of Geophysics, 55(3), 719-778.

Hu, X., Sun, J., Xia, C., Shen, X., Zhang, Y., Liu, Q., ... & Zhang, X. (2023). Measurement report: Rapid decline of aerosol absorption coefficient and aerosol optical property effects on radiative forcing in an urban area of Beijing from 2018 to 2021. Atmospheric Chemistry and Physics, 23(9), 5517-5531.

IPCC, 2023: Climate Change 2023: Synthesis Report. Contribution of Working Groups I, II and III to the Sixth Assessment Report of the Intergovernmental Panel on Climate Change [Core Writing Team, H. Lee and J. Romero (eds.)]. IPCC, Geneva, Switzerland, pp. 35-115, doi: 10.59327/IPCC/AR6-9789291691647.

Jacobson MZ (2002) Control of fossil-fuel particulate black carbon and organic matter, possibly the most effective method of slowing global warming. J Geophys Res Atmos 107(D19): ACH-16.

Jie Z et al (2017) Validation of MODIS C6 AOD products retrieved by the dark target method in the Beijing–Tianjin–Hebei urban agglomeration, China. Adv Atmos Sci 34:993–1002.

Jin, Q., Wei, J., Lau, W. K., Pu, B., & Wang, C. (2021). Interactions of Asian mineral dust with Indian summer monsoon: Recent advances and challenges. Earth-Science Reviews, 215, 103562.

Jing W, Lin S, Bo H, Bilal M, Wang L (2018) Verification, improvement and application of aerosol optical depths in China. Part 1: inter-comparison of NPP-VIIRS and Aqua-MODIS. Atmos Environ 175:221–233.

Kaufman, Y. J., Gitelson, A., Karnieli, A., Ganor, E., Fraser, R. S., Nakajima, T., ... & Holben, B. N. (1994). Size distribution and scattering phase function of aerosol particles retrieved from sky brightness measurements. Journal of Geophysical Research: Atmospheres, 99(D5), 10341-10356.

Kumar RP, Perumpully SJ, Samuel C, Gautam S (2022b) Exposure and health: a progress update by evaluation and scientometric analysis. Stoch Environ Res Risk Assess. https:// doi. org/ 10. 1007/ s00477-022-02313-z.

Lillis D, Cruz CN, Collet J Jr, Richards LW, Pandas SN (1999) Production and removal of aerosol in a polluted fog layer: model evaluation and fog effect on PM. Atmos Environ 33(29):4797–4816.

Li, Y., Wang, T., Wang, Q. G., Li, M., Qu, Y., Wu, H., ... & Xie, M. (2024). Deciphering the seasonal dynamics of multifaceted aerosol-ozone interplay: Implications for air quality management in Eastern China. Science of The Total Environment, 946, 174327.

Mahowald N, Albani S, Kok JF, Engelstaeder S, Scanza R, Ward DS, Flanner MG (2014) The size distribution of desert dust aerosols and its impact on the Earth system. Aeol Res 15:53–71.

Masood, A., Zhu, F. R., Sa'adi, Z., Mamun Hridoy, M. A. A., & Ullah, I. (2025). Study of meteorological parameters and classification of aerosols using remote sensing over LHAASO. Theoretical and Applied Climatology, 156(7), 375.

Park T, Liu MY, Wang TC, Zhu JY (2019) Semantic image synthesis with spatially-adaptive normalization. In: Proceedings of the IEEE/CVF conference on computer vision and pattern recognition, p 2337–2346.

Perumpully, S. J., & Gautam, S. (2024). Impact of aerosols on atmospheric processes and climate variability: A synthesis of recent research findings. Geosystems and Geoenvironment, 100317.

Pu, B., & Ginoux, P. (2018). Climatic factors contributing to long-term variations in surface fine dust concentration in the United States. Atmospheric Chemistry and Physics, 18(6), 4201-4215.

Perumpully, S. J., Gautam, S., & M, S. (2024). Evaluating the impact of personal exposure to emissions from sustainable commercial heating and cooking fuels on women in Rural Southern India and their alignment with sustainable development goals. Water, Air, & Soil Pollution, 235(1), 54.

Perumpully, S. J., & Gautam, S. (2025). Impact of aerosols on atmospheric processes and climate variability: A synthesis of recent research findings. Geosystems and Geoenvironment, 4(1), 100317.

Ramachandran S, Rengarajan R, Jayaraman A, Sarin MM, Das SK (2006) Aerosol radiative forcing during clear, hazy, and foggy conditions over a continental polluted location in north India. J Geophys Res Atmos. https:// doi. org/ 10. 1029/ 2006J D0071 42.

Ranjan RR, Joshi HP, Iyer KN (2007) Spectral variation of total column aerosol optical depth over Rajkot: a tropical semi-arid Indian station. Aerosol Air Qual Res 7(1):33–45.

Ren, X., Wu, J., Gong, C., Gao, W., Zhao, D., Ma, Y., & Xin, J. (2022). The relationship between PM2. 5 pollution and aerosol radiative forcing in a heavy industrial city, Taiyuan, in China. Atmospheric Research, 267, 105935.

Ruiz-Arias, J. A., Gueymard, C. A., Quesada-Ruiz, S., Santos-Alamillos, F. J., & Pozo-Vázquez, D. (2016). Bias induced by the AOD representation time scale in long-term solar radiation calculations. Part 1: Sensitivity of the AOD distribution to the representation time scale. Solar Energy, 137, 608-620.

Satheesh SK, Ramanathan V (2000) Large differences in tropical aerosol forcing at the top of the atmosphere and Earth's surface. Nature 405(6782):60–63.

Singh, P., Vaishya, A., Rastogi, S., & Babu, S. S. (2020). Seasonal heterogeneity in aerosol optical properties over the subtropical humid region of northern India. Journal of Atmospheric and Solar-Terrestrial Physics, 201, 105246.

Solomon, P., Cowling, E., Hidy, G., & Furiness, C. (2000). Comparison of scientific findings from major ozone field studies in North America and Europe. Atmospheric Environment, 34(12-14), 1885-1920.

Stirnberg, R., Cermak, J., & Andersen, H. (2018). An analysis of factors influencing the relationship between satellite-derived AOD and ground-level PM10. Remote Sensing, 10(9), 1353.

Tao, M., Chen, L., Wang, Z., Wang, J., Che, H., Xu, X., ... & Hou, C. (2017). Evaluation of MODIS Deep Blue aerosol algorithm in desert region of East Asia: Ground validation and intercomparison. Journal of Geophysical Research: Atmospheres, 122(19), 10-357.

Tian X, Liu Q, Li X, Wei J (2018) Validation and comparison of MODIS C6.1 and C6 aerosol products over Beijing. China. Remote Sens 10:2021.

Wang, L., Xin, J., Wang, Y., Li, Z., Liu, G., & Li, J. (2007). Evaluation of the MODIS aerosol optical depth retrieval over different ecosystems in China during EAST-AIRE. Atmospheric Environment, 41(33), 7138-7149.

Wang, P. X., Wang, B., Cheng, H., Fasullo, J., Guo, Z. T., Kiefer, T., & Liu, Z. Y. (2014). The global monsoon across timescales: coherent variability of regional monsoons. Climate of the Past, 10(6), 2007-2052.

Wang Y, Yuan Q, Li T, Shen H, Zheng L, Zhang L (2019) Evaluation and comparison of MODIS Collection 6.1 aerosol optical depth against AERONET over regions in China with multifarious underlying surfaces. Atmos Environ 200:280–301.

Xie, Y., Zhang, Y., Xiong, X., Qu, J. J., & Che, H. (2011). Validation of MODIS aerosol optical depth product over China using CARSNET measurements. Atmospheric Environment, 45(33), 5970-5978.

Yang, L., Tian, X., Liu, C., Ji, W., Zheng, Y., Liu, H., ... & Che, H. (2022). Evaluation and comparison of MODIS C6 and C6. 1 deep blue aerosol products in arid and semi-arid areas of northwestern China. Remote Sensing, 14(8), 1935.

Yoon, J., von Hoyningen-Huene, W., Kokhanovsky, A. A., Vountas, M., & Burrows, J. P. (2012). Trend analysis of aerosol optical thickness and Ångström exponent derived from the global AERONET spectral observations. Atmospheric Measurement Techniques, 5(6), 1271-1299.

Zhang MM, Liu ZB, Yun-Jian GE, Basin EY (2014a) Spatio-temporal distribution of atmospheric aerosol optical depth in Jiangsu Province.

Zhang M, Gong W, Zhu Z (2014b) Aerosol optical properties of a haze episode in Wuhan based on ground-based and satellite observations. Atmosphere 5:699–719.

Zhao, S., Hu, B., Du, C., Tang, L., Ma, Y., Liu, H., ... & Wang, Y. (2019). Aerosol optical characteristics and radiative forcing in urban Beijing. Atmospheric Environment, 212, 41-53.

Zhao, S., Liu, M., Tao, M., Zhou, W., Lu, X., Xiong, Y., ... & Wang, Q. (2023). The role of satellite remote sensing in mitigating and adapting to global climate change. Science of the Total Environment, 166820.